

Research Articles | Development/Plasticity/Repair

Vesicular glutamate release is necessary for neural tube formation

<https://doi.org/10.1523/JNEUROSCI.0681-25.2026>

Received: 4 April 2025

Revised: 24 January 2026

Accepted: 1 February 2026

Copyright © 2026 Goyal et al.

This is an open-access article distributed under the terms of the [Creative Commons Attribution 4.0 International license](#), which permits unrestricted use, distribution and reproduction in any medium provided that the original work is properly attributed.

This Early Release article has been peer reviewed and accepted, but has not been through the composition and copyediting processes. The final version may differ slightly in style or formatting and will contain links to any extended data.

Alerts: Sign up at www.jneurosci.org/alerts to receive customized email alerts when the fully formatted version of this article is published.

1 **Vesicular glutamate release is necessary for neural tube formation**

2
3
4 Abbreviated title: Mechanism of glutamate release from the neural plate

5
6
7 Raman Goyal¹, Patricio A. Castro^{1,2}, Jacqueline B. Levin¹, Sangwoo Shim¹, Olga A. Balashova¹,
8 Alexios A. Panoutsopoulos¹, Nicolas A. Fuentes², Grace Or Mizuno³, Lin Tian^{3,4}, Laura N.
9 Borodinsky^{1,5}

10
11
12 ¹Department of Physiology & Membrane Biology, Shriners Hospitals for Children Northern
13 California, University of California Davis, School of Medicine, Sacramento, CA, USA.

14 ²Laboratory of Neural Development, LAND, Departamento de Fisiología, Facultad de Ciencias
15 Biológicas, Universidad de Concepción, Concepción 4030000, Chile.

16 ³Department of Biochemistry & Molecular Medicine, University of California Davis, School of
17 Medicine, Sacramento, CA, USA.

18
19
20 ⁴Present address: Max Planck Florida Institute for Neuroscience, USA

21 ⁵Corresponding author. Email: lnborodinsky@ucdavis.edu

22
23
24 Number of pages: 38

25 Number of figures: 6

26 Number of words: Abstract – 155

27 Introduction – 647

28 Discussion – 947

29
30 **Conflict of interest declaration**

31 The authors declare no competing financial interests.

32

33 **Acknowledgments**

34 This work was supported by: National Science Foundation grant 1754340 (LNB) and while serving
35 as Program Director for NSF under IPA agreement (LNB), National Institutes of Health grants
36 R01NS105886 and R01NS113859 (LNB), Shriners Hospital for Children grant 85111 (LNB) and
37 grant 84303 (RG) and Fondo Nacional de Desarrollo Científico y Tecnológico, Chile grant
38 1231038 (PAC).

39

40

41

42

43

44

45

46 **Abstract**

47 The brain and spinal cord originate from a neural tube that is preceded by a flat structure known
48 as the neural plate during early embryogenesis. In humans, failure of the neural plate to convert
49 into a tube by the fourth week of pregnancy leads to neural tube defects (NTDs), birth defects
50 with serious neurological consequences. The signaling mechanisms governing the process of
51 neural tube morphogenesis are unclear. Here we show that in *Xenopus laevis* embryos glutamate
52 is released during neural plate folding in a Ca^{2+} and vesicular glutamate transporter-1 (VGLUT1)-
53 dependent manner. Vesicular release of glutamate elicits Ca^{2+} transients in neural plate cells that
54 correlate with activation of Erk1/2. Knocking down or out VGLUT1, globally or neural tissue-
55 specifically, leads to NTDs and increased expression of Sox2, neural stem cell transcription factor,
56 and neural plate cell proliferation. Exposure during early pregnancy to neuroactive drugs that
57 disrupt these signaling mechanisms might increase the risk of NTDs in offspring.

58

59

60 **Significance Statement**

61 Neural tube defects are serious and common birth defects that occur when the neural tube fails
62 to form and close at four weeks of pregnancy. Use of antiepileptic drugs during early pregnancy
63 increases the risk of these defects by unclear mechanisms. Here we show that vesicular release
64 of glutamate occurs during and is necessary for neural tube formation in *Xenopus laevis* embryos.
65 This study motivates discussion on the presynaptogenic signaling mechanisms in the nervous
66 system and their role during these early developmental stages, challenging the prevailing
67 paradigm that neurotransmission is not apparent until neurons fully differentiate and synapses
68 are formed.

JNeurosci Accepted Manuscript

69 Introduction

70 One of the first steps in nervous system development is the formation of the neural tube, which
71 constitutes the presumptive brain and spinal cord, that originates from a flat layer of
72 neuroectodermal stem cells called the neural plate. Failure in neural tube morphogenesis leads
73 to birth defects known as neural tube defects (NTDs) that can be lethal or result in various
74 neurological disabilities (Wallingford et al., 2013; Nikolopoulou et al., 2017).

75 The cellular events that are required for the morphogenesis of the neural tube include apical
76 constriction of neural plate cells to enable bending, dorsoventral cell elongation to facilitate the
77 curvature needed for the reshaping of the tissue, cell intercalation to enable the process of
78 convergent extension, and cell migration towards the midline for fusion and closure of the neural
79 tube (Ybot-Gonzalez and Copp, 1999; Ybot-Gonzalez et al., 2002; Haigo et al., 2003; Park et al.,
80 2005; Lee and Harland, 2010; Ossipova et al., 2014; Nikolopoulou et al., 2017). In addition, the
81 role of cell proliferation in neural tube formation has been a subject of extensive investigation
82 (Jelínek and Fribová, 1966; Copp et al., 1988a; Harris and Hartenstein, 1991; Leise and Mueller,
83 2004; Ciruna et al., 2006; McShane et al., 2015; Parchem et al., 2015; Yang et al., 2015;
84 Herrlinger et al., 2019; Pokrovsky et al., 2021). These studies show that increase or decrease in
85 neuroepithelial cell proliferation can lead to NTDs in various species. Interestingly, in *Xenopus*
86 *laevis* embryos, blocking cell proliferation following gastrulation does not interfere with neural tube
87 closure (Harris and Hartenstein, 1991; Pokrovsky et al., 2021). In contrast, inhibiting cell cycle
88 progression in embryos in which genetic (curly tail mouse; (Copp et al., 1988b)) or
89 pharmacological (valproic acid-incubated *Xenopus laevis* embryo; (Sequera et al., 2018))
90 perturbations induced imbalanced neural plate cell proliferation, partially rescues the NTD
91 phenotype. Overall, these studies suggest that precise regulation of cell proliferation is important
92 for the morphogenesis of the neural tube.

93 Although several molecules that participate in these cellular events have been identified, the
94 signaling mechanisms that operate in neural plate cells are unclear.

95 The causes of NTDs appear to be both genetic and environmental. Antiepileptic drugs are
96 considered a risk factor for NTDs (Nakane et al., 1980; Lindhout et al., 1992; Omtzigt et al., 1992;
97 Kaneko et al., 1999; Werler et al., 2011; Wlodarczyk et al., 2012). Although the prevailing view
98 has been that these drugs interfere with neural tube morphogenesis through off-target effects
99 (Eyal et al., 2004), our previous study has demonstrated that valproic acid, a commonly used
100 antiepileptic drug, induces NTDs in frog embryos by a similar cellular mechanism as interfering
101 with NMDA receptor-dependent glutamate signaling, which perturbs regulation of neural plate cell
102 proliferation. Moreover, valproic acid-induced NTDs are partially rescued not just by inhibiting cell
103 proliferation, but also by enhancing glutamate signaling (Sequerra et al., 2018). These studies
104 suggest that the regulation of cell proliferation that is important for neural tube folding is dependent
105 on glutamate signaling.

106 The mechanism by which glutamate is released in a developmental stage when neurons are not
107 yet fully differentiated, and synapses are not formed is unclear. Synaptic glutamate release is
108 dependent on the expression and compartmentalization of key molecules that participate in the
109 storing of glutamate in synaptic vesicles, anchoring of vesicles in synaptic terminals, fusion of
110 vesicles and release of neurotransmitter (Zhou and Danbolt, 2014). Prominently, vesicular
111 glutamate transporters are indispensable for filling synaptic vesicles with glutamate in
112 glutamatergic synapses (Hackett and Ueda, 2015). Whether aspects of the mechanism of
113 vesicular glutamate release in synapses are also recruited at the early stages of neural plate
114 folding has never been investigated before.

115 Here we show that the vesicular glutamate transporter 1 (VGluT1) is expressed in the neural plate
116 and is necessary for neural tube formation. This study demonstrates VGluT1-dependent release

117 of glutamate that mediates Ca^{2+} dynamics to regulate neural plate cell proliferation and
118 morphogenesis of the neural tube.

JNeurosci Accepted Manuscript

119 **Materials and Methods**

120 **Animals**

121 All experimental procedures and research design utilized in this study complied with ethical
122 regulations. The Institutional Animal Care and Use Committee approved the animal protocol
123 #22264 implemented in this study. IACUC follows the guidelines established by the Animal
124 Welfare Act and the Public Health Service Policy on Humane Care and Use of Laboratory
125 Animals.

126

127 ***Xenopus laevis* animal handling and *in vitro* fertilization**

128 Mature oocytes were collected in a dish from a previously hCG injected female frog and incubated
129 with a small piece of minced testis. This is considered time 0 of fertilization. Fertilized oocytes
130 were kept in 10% MMR saline, containing (in mM): 10 NaCl, 0.2 KCl, 0.1 MgSO₄, 0.5 Hepes, 5
131 EDTA and 0.2 CaCl₂. Dejelling of embryos was done by briefly swirling fertilized eggs in 2%
132 cysteine solution, pH 8. Developmental stages were recorded according to Nieuwkoop and Faber
133 (Nieuwkoop and Faber, 1994). Animals were handled according to the IACUC guidelines using
134 humane procedures to prevent animal suffering.

135

136 **Gene expression assays**

137 Neural plates from 9 mid neural plate stage (stage 16) *Xenopus laevis* embryos were isolated by
138 incubating dorsal halves of embryos with 1 mg/ml collagenase for 1 min. This allows to dissect
139 out the neural plate from mesodermal and endodermal tissues. Dissected neural plates were then
140 resuspended in Trizol reagent (Invitrogen, cat. # 15596026) and stored at -80°C. RNA was
141 extracted with kit according to manufacturer's instructions (RNeasy Mini Kit, Qiagen, cat. #

142 74104), gDNA was eliminated (RapidOut DNA Removal Kit, Thermo Scientific, cat. # 00859896)
143 and cDNA was made (High-Capacity cDNA Reverse Transcription Kit, Applied Biosystems, cat.
144 # 00890068) with standard protocols. Using this cDNA as template, RT-PCR was performed with
145 the following primers: vesicular glutamate transporter 1 (*vglut1*): forward,
146 GCAACTTGGGTGTAGCCATT, reverse, TGCCATTTACTCCAGATCC; excitatory amino acid
147 transporter 5 (*eaat5*): forward, GTGGGATGTCTGCTTGGATT, reverse,
148 ATGTGGCTTCCACAAGGTTTC; syntaxin 1A (*stx1a*): forward, ATGAAGGATCGGACCAGGGA,
149 reverse, TGTGGCGTTGTATTCGGACA; vesicle associated membrane protein 1 (*vamp1*):
150 forward, GCCACAGGTGATCCTGGAAA, reverse, AGGAGACGCTCCACACAATG;
151 synaptosome associated protein 25 (*snap25*) forward, AAGGCTTGGGGCAATAACCA, reverse,
152 AACCACTGCCCAGCATCTTT, designed using Primer-BLAST (www.ncbi.nlm.nih.gov). All
153 sequences are written from 5' to 3'.

154 Quantitative RT-PCR for assessment of developmental *vglut1* expression and comparison of
155 *vglut1*, *vglut2* and *vglut3* was performed by homogenizing embryos in Trizol reagent (Invitrogen,
156 cat. # 15596026) and storing samples at -80 °C. RNA was extracted with kit according to the
157 manufacturer's instructions (RNeasy Mini Kit, Qiagen, cat. # 74104), gDNA was eliminated
158 (RapidOut DNA Removal Kit, Thermo Scientific, cat. # 00859896) and cDNA was made (High
159 Capacity cDNA Reverse Transcription Kit, Applied Biosystems, cat. # 00890068) with standard
160 protocols. Using cDNA as template, qRT-PCR was performed with SYBR Green Universal Master
161 Mix (Applied Biosystems, cat. # 2107118) in the Stratagene Mx3005 real-time PCR machine. RT-
162 PCR program: 15 min 95 °C, 50 cycles of 45 s at 95 °C/30 s at 47 °C/ 30 s at 72 °C, 1 min at 95
163 °C, 30 s at 47 °C, and 30 s at 95 °C. Primers used were: *vglut1*, forward:
164 CCACGGGATCTGGAGTAAATG, reverse: CTGAACTCCACCCAGAGTATTG; or forward:
165 TACTACTAGGACGTCTGCACAGGAT, reverse: CGAGGAAGCCCAAAGCAAGTACAA; *odc*,
166 forward: GTCAATGATGGAGTGTATGGATC, reverse:

167 TCCATTCCGCTCTCCTGAGCAC; *vglut2*, forward: GCAGGAGCTGTTATTGCTATGCCA,
168 reverse: GAAGAGGTACCAAACCAGGCCAAA; *vglut3*, forward:
169 TCAGACTCAGCCACCTCCAAGATT, reverse: ATGCAAAACCCCAAGCCACTCA; *sub1*,
170 forward: CAACTGAAGGAGCAGATGTCGGAT, reverse: CATGGTTTCGTCAAGGCGTAGGTA.
171 All sequences are written from 5' to 3'.

172

173

174 **VGluT1 knockdown**

175 Two-cell-stage embryos were unilaterally or bilaterally injected with 2-8 pmol of translation
176 blocking morpholino (MO) VGluT1-MO1 TCCTAAACTCCATTGTGATCCTCCT (VGluT1-
177 KD1/KD) or with 8 pmol splicing blocking MO (VGluT1-KD2) VGluT1-MO2
178 ATGTTTTTTCCTTACCTCGATAACA per blastomere (Gene Tools, Inc). Controls were sibling
179 embryos injected with standard control MO, CCTCTTACCTCAGTTACAATTTATA (Control).
180 Morpholinos were injected along with dextran-Alexa-Fluor conjugates or with GFP or mCherry
181 mRNA to assure permanency of MO reporter after PFA or TCA fixation. All sequences are written
182 5' to 3'. Rescue experiments were implemented by injecting 250 pg of VGluT1-MO-resistant
183 *Xenopus laevis vglut1*- mRNA (125 pg/blastomere) along with VGluT1-MO. *X. laevis* VGluT1
184 mRNA was modified by substitution of 5' UTR with a fragment of the Kozak consensus sequence
185 gcc acc (Kozak, 1987). A number of wobble mutations were introduced in the VGluT1 coding
186 region to prevent VGluT1-MO binding to modified *vglut1* mRNA. mRNA was synthesized as
187 previously described (Borodinsky et al., 2004a; Belgacem and Borodinsky, 2011; Swapna and
188 Borodinsky, 2012; Balashova et al., 2017). Assessment of VGluT1-KD efficiency was performed
189 by Western blot and PCR assays (splicing-blocking MO).

190 Assessment of VGlut1 splicing blocking MO (MO2) efficiency was performed by homogenizing 9
191 stage 15 embryos in each group in Trizol reagent (Invitrogen, cat. # 15596026). Samples were
192 stored at -80°C . RNA was extracted with kit according to manufacturer's instructions (RNeasy
193 Mini Kit, Qiagen, cat. # 74104), gDNA was eliminated (RapidOut DNA Removal Kit, Thermo
194 Scientific, cat. # 00859896) and cDNA was made (High-Capacity cDNA Reverse Transcription
195 Kit, Applied Biosystems, cat. # 00890068) with standard protocols. Using this cDNA as template,
196 PCR was performed for Control-MO and VGlut1-MO2 injected embryos with primers located in
197 exon 1 and exon 2 that generates no PCR product from cDNA of non-spliced *vglut1* transcript
198 and a 100 bp PCR product when the mRNA is spliced correctly (MO control). Forward primer:
199 GCATGGTCAACAACAACACG, Reverse primer: GAACCGTGTATCATGCCGAC, written from 5'
200 to 3'.

201

202 **Western blot assays**

203 To determine VGlut1 and Sox2 protein levels, neural tube, stage-22 whole embryos were
204 homogenized in extraction buffer containing 1% Triton X-100, 150 mM NaCl, 25 mM Hepes pH
205 7.4, 2 mM EDTA and protease inhibitors cocktail (Thermo Fisher Scientific). Samples were
206 centrifuged at 16,100 *g* for 10 min and the pellet discarded. Supernatant was then boiled with
207 Laemmli buffer and run on a 10% SDS-PAGE followed by protein transfer to PVDF membrane.
208 PVDF membranes were probed with monoclonal anti-*Xenopus*-VGlut1 1:500 (Genescript,
209 costume-made) 5% milk, Sox2 1:500 (catalog# AF2018 R&D Systems) in 5% BSA followed by
210 incubation with HRP-conjugated secondary antibodies 1:10,000 (Jackson ImmunoResearch) and
211 visualized by Western Lightning Plus-ECL, Enhanced Chemiluminescence Substrate (catalog#
212 NEL103E001, PerkinElmer). PVDF membranes were stripped in 0.2 M glycine HCl buffer, pH 2.5,
213 0.05% Tween for 20 min and reprobed with GAPDH 1:50,000 in 5% Milk (catalog# 60004-1-1g
214 Proteintech), as loading control, followed by incubation with HRP-conjugated secondary

215 antibodies 1:20,000 (Jackson ImmunoResearch) and visualized by Western Lightning ECL
216 (Millipore/Sigma, cat. # GERPN2106).

217

218 **Whole-mount immunostaining**

219 Embryos at stage 13 through 18 were fixed in 4% PFA for 2 h at 23°C or overnight at 4°C and the
220 dorsal half containing the neural plate was isolated and bleached in 1:2 Dent's fixative/H₂O₂
221 overnight at 23°C. Samples were washed, permeabilized in 1% Triton-X100, and incubated
222 overnight at 4°C with primary antibodies, followed by staining with fluorescent secondary
223 antibodies at 23°C for 2 h, and finally clearing overnight in benzyl benzoate. Z-stack confocal
224 images of embryos or neural tissue (100 μm-thick) were taken with a confocal microscope (Nikon
225 C1 or C2), 10X or 20X objective, through approximately 30-100 steps (3-10 μm) longitudinally
226 through a dorsoventral direction. Primary antibodies used for whole mount immunostaining were:
227 VGlut1 1:200 (catalog # AB5905, EMD-Millipore), Sox2 1:200 (catalog # AF2018, R&D Systems),
228 pERK1/2 1:200 (catalog # 4377S, Cell Signaling Technology), PCNA 1:1,000 (catalog # 2586S,
229 Cell Signaling Technology), PHH3 1:500 (catalog #06-570, EMD Millipore), and GFP 1:500
230 (catalog # ab13970 Abcam).

231 Quantitative assessment of the number of cells immunopositive for VGlut1, Sox2, PCNA and
232 PHH3 was performed by using the Imaris 'Spot' function to detect nuclei objects filtered by object
233 size, fluorescence intensity, and the built-in quality threshold.

234

235 **Immunohistochemistry of tissue sections**

236 Neural plate stage embryos were fixed at 23°C with 4% PFA for 10 min, and processed for
237 immunostaining as previously described (Balashova et al., 2017). Briefly, samples were paraffin-

238 embedded and 10 mm-thick transverse sections of the neural plate were incubated with primary
239 and secondary antibodies overnight at 4°C and for 2 h at 23°C, respectively. Primary antibodies
240 used were: VGluT1/2 (SYSY, 1:1,000), b-tubulin (E7, 1:100, DSHB), and Myc-tag 1:2,000
241 (catalog # 2276, Cell Signaling). Antigen retrieval was performed by boiling samples in 0.05%
242 citraconic anhydride or in Diva antigen retrieval solution (Biomedical Care), pH 7.4 for 10 min in
243 water bath. Samples were permeabilized with PBST (0.5% Triton) for 1 h at 23°C, blocked with
244 5% BSA in PBST (0.1% Triton) for 30 min using SNAP i.d. 2.0 System for immunohistochemistry
245 (Millipore). Samples were imaged with a confocal microscope (Nikon A1), 60X objective through
246 approximately 15 1-mm steps.

247

248 **Electron Microscopy**

249 Transmitted EM

250 Embryos were fixed in 3% glutaraldehyde in 100 mM HEPES (pH 7.4) overnight at 4°C and
251 washed several times in 100 mM HEPES and processed for routine TEM. Specimens were
252 postfixed in 1% OsO₄ in PBS overnight on ice and washed in PBS and water. Fixed embryos
253 were embedded in epoxy blocks. Ultrathin sections were stained with uranyl acetate and lead
254 citrate prior to viewing on a transmission electron microscope (Philips CM120 Biotwin Lens, FEI
255 Company) using a Gatan MegaScan digital camera (model 794/20, 2K × 2K, Gatan).

256 Immuno-TEM

257 Embryos were fixed in 4% paraformaldehyde in 0.1 M sodium phosphate buffer at 4°C overnight.
258 Ultrathin sections were incubated with primary and secondary antibodies overnight at 4°C and for
259 2 h at 23°C, respectively. Primary antibody was VGluT1 1:100-1:10,000 (catalog # AB5905, EMD-
260 Millipore). Secondary antibody was goat-anti-guinea pig IgG, EM grade, 10 nm 1:40 (catalog #

261 25329, Electron Microscopy Sciences). Immunolabeled sections were imaged on the same
262 electron microscope as indicated before. Control samples consisted in embryos and ultrathin
263 sections subjected to the same procedure except omission of primary antibody.

264

265 **Measurement of glutamate release**

266 iGluSnFR

267 Two-cell stage wild type and unilaterally injected with 2 pmol VGluT1-MO1 or Control-MO+Alexa
268 647-dextran embryos were bilaterally injected with 8 ng iGluSnFR mRNA per embryo [iGluSnFR,
269 a modified (pcDNA-spacer-123D5, Lin Tian's Lab) derived from construct gift from Loren Looger,
270 Addgene plasmid # 41732, (Marvin et al., 2013)] that was previously subcloned into the pCS2⁺
271 vector. iGluSnFR-expressing stage 13-16 embryos were confocally time-lapse imaged at 1 Hz
272 acquisition rate. Images were taken at different neural plate stages using Nikon confocal
273 microscope in response to 2-5 mM ionomycin or DMSO for 5 min followed by 5 mM glutamate.
274 Membrane-mCherry expressing embryos were used as controls. Fluorescence intensity was
275 measured using NIS Elements software.

276 Fluorometric assay

277 Neural plate stage (stage 15-15.5) wild type and morpholino-injected embryos were incubated
278 with 100 nM tetanus toxin or DMSO for 1 h followed by 1 h incubation with 2 mM ionomycin in
279 200 ml volume. Bathing solution was collected and released glutamate measured with a
280 Fluorometric Glutamate Assay Kit (STA-674 Cell-biolabs).

281

282 **In vivo Ca²⁺ imaging**

283 DNA encoding the Ca²⁺ sensor GCaMP6s (pGP-CMV-GCaMP6s, a gift from Douglas Kim, HHMI
284 Janelia Research Campus, Ashburn, Virginia; plasmid #40753, Addgene; (Chen et al., 2013))
285 was subcloned into the pCS2⁺ vector using BglII and NotI restriction sites. The BglII restriction site
286 was included in pCS2⁺ with the following primers: forward, 5' -
287 TCACTAAAGGGAACAAAAGATCTGGGTACCGGGCCCAA-3'; reverse, 5' -
288 TTGGGCCCGGTACCCAGATCTTTTGTTCCTTTAGTGA-3'. For all experiments in this study,
289 mRNA was transcribed from the indicated plasmids using mMessage mMachine kits (Ambion).
290 GCaMP6s mRNA was injected in two-cell-stage embryos (1 ng mRNA/embryo). Neural plate
291 stage embryos [14 –19 h postfertilization (hpf)] were imaged under a confocal microscope at an
292 acquisition rate of 0.05-0.1 Hz for 5 min to 2 h. Detection of Ca²⁺ transients was thresholded by a
293 peak change in fluorescence of at least 2 times the noise, as in previous studies (Borodinsky et
294 al., 2004b; Belgacem and Borodinsky, 2011; Swapna and Borodinsky, 2012). The number of Ca²⁺
295 transients in unilaterally VGlut1-KD1 or Control embryos were compared, and significance was
296 assessed by paired t test.

297

298 **Imaging of Erk1/2 activity**

299 piRFP670 (a gift from Vladislav Verkhusha; Addgene plasmid # 45457; (Shcherbakova and
300 Verkhusha, 2013)) was subcloned into pCS2⁺ using KpnI and NotI (New England Biolabs; NEB).
301 The ERK-sensitive region of ERKTRClover from pENTRA-ERKTRClover (a gift from Markus
302 Covert; Addgene plasmid # 59138; (Regot et al., 2014)) was removed and amplified by PCR using
303 the following primers: forward: CAAAGGTACCGGCAACATGGCAAAGGGCCGAAAGCC,
304 reverse: CACCATACCGGTGAGGATGGGAATTG. These primers add KpnI and AgeI restriction
305 sites, keep the iRFP in frame with the KTR, and optimize the Kozak sequence of the new construct
306 for *Xenopus laevis* expression (Kozak, 1991; Nakagawa et al., 2007). The PCR product and
307 piRFP670-pCS2⁺ were both digested with KpnI and AgeI (NEB), gel purified, and ligated. The

308 new plasmid was confirmed by restriction digests and RNA was made from the T3 promoter using
309 Ambion's mMessage mMachine kit. The sensitivity of the new construct was confirmed in culture
310 as described below using phorbol 12-myristate 13-acetate (PMA; agonist) or PD0325901
311 (antagonist).

312 Embryos were injected at the 2-cell-stage with a mixture of mRNA encoding GCaMP6s (1.5 ng),
313 ERK-KTR-iRFP670 (1.5 ng), and H2B-mRFP1 (200 pg; mRNA made from the SP6 promoter of
314 pCS2⁺-H2B-mRFP1, a gift from Sean Megason; Addgene plasmid # 53745), or 2 pmol VGluT1-
315 MO or Control-MO (unilateral; along with tracer), 1.5 ng ERK-KTR-iRFP670 (bilateral), and 200
316 pg H2B-mRFP1 (bilateral). They were grown at 18-21°C until early neural plate stages when they
317 were confocally imaged in the 3 channels.

318 For simultaneous Ca²⁺ and Erk1/2 activity analysis, nuclei were tracked by H2B signal in NIS
319 Elements software (Nikon) and the intensity of all three channels in this H2B-RFP-fluorescently-
320 labeled area (nuclear) and surrounding area (cytosolic) over time were measured. Cells were
321 categorized into Ca²⁺-active or Ca²⁺-silent based on occurrence of Ca²⁺ transients or not during
322 the recording, respectively. At least 5 cells of each category were analyzed per embryo (total: 70
323 cells). Ca²⁺ active cells were first selected and Ca²⁺-silent cells were sampled to match
324 anteroposterior and mediolateral contralateral localization to those active in each embryo.
325 Average of cytosolic/nuclear ERK-KTR-iRFP670 was calculated per group per embryo and
326 comparisons were performed with paired t-test.

327 For assessing Erk1/2 activity dependence on VGluT1 expression we imaged embryos at mid-
328 neural plate stages (stage 15-16) and measured ERK-KTR-iRFP670 cytosolic/nuclear signal in
329 cells of VGluT1-MO/Control-MO injected and wild type halves of neural plate. Cells were sampled
330 to match anteroposterior and mediolateral localization across groups. Average of
331 cytosolic/nuclear ERK-KTR-iRFP670 of at least 5 cells in each half of the neural plate from at

332 least 4 embryos (total neural plate cells at least 40) was calculated per wild type and injected
333 neural plate per embryo and comparisons were performed with paired t-test.

334

335 **VGluT1 knockout**

336 Synthetic guidance RNA (sgRNA) targeting *vglut1* was designed using the CRISPRscan website
337 (Moreno-Mateos et al., 2015), and inDelphi model (Shen et al., 2018), which provide in silico
338 predictions for mutational outcomes. The VGluT1 sgRNA (guidance sequence:
339 AGCCTGCTACGCTCCAGAGG) was synthesized using the EnGen sgRNA synthesis kit (New
340 England Biolabs). The sgRNA was complexed with Cas9 protein (PNA Bio, #CP02) at 300 mM
341 KCl to form ribonucleoprotein complexes and injected into embryos. The CrispantCal web tool
342 (Burger et al., 2016) was used to calculate volumes corresponding to an optimal one-to-one
343 molecular ratio of gRNA to Cas9 in a CRISPR-Cas9 injection mix. To quantify the editing
344 efficiency, genomic DNA was extracted from 5 edited embryos at early neural plate stages (stage
345 14) using DNeasy Blood & Tissue Kit (Qiagen). The edited locus of *vglut1.s* was amplified from
346 genomic DNA using primers, forward, 5'-TTTGCGCTTGACCCAGGTAT-3'; reverse, 5'-
347 ACGGGCGACAATTTTATGCG-3', specific to the CRISPR/Cas9-targeted site for Sanger
348 sequencing. The sequencing results were used for in silico analysis of the INDELS generated by
349 the CRISPR/Cas9-mediated editing using Inference of CRISPR Edit analysis software
350 (Synthego).

351

352 **Neuroectoderm-specific VGluT1 knockdown**

353 Eight-cell-stage embryos were bilaterally injected with 2 pmol of translation blocking morpholino
354 (MO) VGluT1-MO1 TCCTAAACTCCATTGTGATCCTCCT (VGluT1-KD1/KD) per dorsal
355 blastomere (Gene Tools, Inc). Controls were sibling embryos injected in dorsal blastomeres with

356 2 pmol standard control MO, CCTCTTACCTCAGTTACAATTTATA (Control). Morpholinos were
357 injected along with dextran-Alexa-Fluor conjugates. All sequences are written 5' to 3'.

358

359 **Assessment of Neural Tube Defect phenotype**

360 VGlut1-KD, VGlut1-KO, Control and vglut1-mRNA injected embryos were imaged with a
361 stereoscope when control embryos reached early neural tube stages (stage 20). Observed
362 phenotypes were categorized in “Closed” or open (“NTDs”) neural tube.

363

364 **Experimental design and statistical analyses**

365 Rigorous research design and analysis was implemented by running all the controls necessary
366 alongside experimental samples. Data analysis was performed blindly by the experimenter or
367 through unbiased automation. Number of samples for each experiment was determined by
368 power analysis of pilot experiments and replicated at least 3 times with at least 5 samples. No
369 data were excluded from the analysis. Statistical analysis of the data was done with Prism
370 software (Graphpad, Inc.). Normality test was performed in each set of data and then parametric
371 (normally distributed) or non-parametric statistical analysis was chosen. Paired tests were
372 implemented in unilaterally manipulated embryos (comparison of non-injected and microinjected
373 halves of neural tissue), or when Ca^{2+} activity or released glutamate (iGluSnFR) was compared
374 before and after addition of an agent in the same sample. Differences were considered statistically
375 different when $p < 0.05$. Exact p values are included in the Source Data File for each data set. Type
376 of statistical test used is indicated in the figure legends.

377

378 **Results**

379 **VGluT1 is expressed in neural plate stage embryos and mediates glutamate release**

380 To investigate the mechanisms of glutamate release in neural plate stages we examined
381 expression of VGluT1, the vesicular glutamate transporter known to be expressed in *Xenopus*
382 *laevis* (Borodinsky et al., 2004a; Root et al., 2008; Session et al., 2016). mRNA expression and
383 Western blot assays show that VGluT1 is expressed in neural plate stages (Figure 1A-E) , in
384 agreement with previous studies (Root et al., 2008), while transcript for the excitatory amino acid
385 transporter 5 (*eaat5*), known to be a retina-specific glutamate transporter (Arriza et al., 1997), is
386 not detected during neural plate stages (Figure 1A). *vglut1* transcript is the most abundant
387 compared with *vglut2* and 3 (Figure 1C), and its expression is upregulated with the progression
388 of neural plate folding (Figure 1D). VGluT1 protein is enriched in neural plate cells (Figure 1F,H)
389 and, similar to transcript levels, the number of VGluT1+/Sox2+ neural plate cells increases as
390 neural plate folding progresses (Figure 1F). The decreased transcript (Figure 1B) and protein
391 (Figure 1E,G) levels when knocking down VGluT1 expression prove the specificity of
392 immunodetection and efficiency of the knockdown approaches used. In addition, transcripts for
393 other proteins associated with neurotransmitter vesicular release, such as syntaxin 1A (*stx1a*),
394 vesicle associated membrane protein 1 (*vamp1*), and synaptosome associated protein 25
395 (*snap25*), are also detected at these neural plate stages (Figure 1A), suggesting that the
396 molecular machinery for vesicular glutamate release is available during neural tube formation.
397 Indeed, ultrastructural assays we performed at these stages show that vesicular structures are
398 prominent in neural plate cells (Figure 1I-I') and that VGluT1 colocalizes in these subcellular
399 compartments (Figure 1J-J'), while control samples, in which VGluT1 antibody was omitted, show
400 no immunogold particles (Figure 1K-K'). This agrees with the pattern of fluorescent
401 immunostaining in neural plate stage embryo transverse sections, where vesicular structures in

402 close proximity to the nucleus of distinct neural plate cells are immunopositive for VGluT1 (Figure
403 1H).

404

405 To determine whether expression of VGluT1 is functional and necessary for glutamate release,
406 we performed live imaging of intact *Xenopus laevis* embryos expressing a genetically encoded
407 sensor of released glutamate, iGluSnFR (123D5-spacer-modified; Lin Tian's lab). We confirmed
408 that the sensor reports levels of extracellular glutamate concentration by adding glutamate to the
409 bathing solution, which results in an increase in iGluSnFR signal (Figure 2A). Results show that
410 the sensor reports a stronger signal in the neuroectoderm compared to the non-neural ectoderm,
411 suggesting higher glutamate release in the neural plate (Figure 2B). In contrast, VGluT1
412 knockdown decreases iGluSnFR signal but not membrane-mCherry fluorescence in the affected
413 neural plate (Figure 2C). This decrease is not due to reduced expression of iGluSnFR because
414 staining for level of expressed reporter (myc-tagged) reveals that expression is comparable in
415 wild type and knockdown halves of neural plate (Figure 2D). These results indicate that VGluT1
416 is expressed and necessary for glutamate release in neural plate stage embryos.

417

418 To further confirm release of glutamate in neural plate stage embryos and determine whether it
419 is dependent on Ca^{2+} influx, as in synapses, we measured in whole live embryos glutamate
420 release in the presence or absence of ionomycin, a Ca^{2+} ionophore, using iGluSnFR (Figure 2E)
421 or a fluorometric ELISA assay (Figure 2F). Results show that Ca^{2+} influx increases glutamate
422 release from neural plate stage embryos (Figure 2E-F), while knocking down VGluT1 expression
423 (Figure 2G) or blocking vesicular neurotransmitter release by pre-incubating neural plate stage
424 embryos with tetanus toxin (Figure 2H) inhibits ionomycin-induced glutamate release (Figure 2G-

425 H). This indicates that mechanisms of Ca²⁺-mediated vesicular glutamate release are present in
426 neural plate stage embryos.

427

428 **VGluT1 is necessary for Ca²⁺ dynamics and signaling in neural plate cells**

429 Neural plate cells exhibit Ca²⁺ transients (Christodoulou and Skourides, 2015; Suzuki et al., 2017;
430 Sequerra et al., 2018) that increase in frequency with the progression of neural plate folding
431 (Sequerra et al., 2018), and are important for the morphogenesis of the neural tube (Christodoulou
432 and Skourides, 2015; Suzuki et al., 2017). The increase in Ca²⁺ transient frequency in the neural
433 plate correlates with progressive increase in the number of VGluT1-expressing neural plate cells
434 (Figure 1C). Hence, we assessed whether VGluT1 regulates neural plate cell Ca²⁺ dynamics. We
435 find that knocking down VGluT1 expression in half of the embryo almost completely abolishes
436 Ca²⁺ transients compared to the counterpart wild type neural plate (Figure 3A), demonstrating a
437 dependence on VGluT1-enabled glutamate signaling for Ca²⁺ dynamics in the neural plate.

438 Glutamate-mediated signaling is known to recruit various Ca²⁺-regulated pathways, including the
439 MAPK cascade (Sweatt, 2004; Thomas and Huganir, 2004). Our previous study demonstrated
440 that NMDA receptor activation elicits Erk1/2 phosphorylation in neural plate cells (Sequerra et al.,
441 2018). We examined the status of Erk1/2 activity in neural plate cells by simultaneously live
442 imaging Erk1/2 and Ca²⁺ activity in intact, neurulating embryos expressing specific, genetically-
443 encoded reporters. We first determined that the Erk1/2 reporter (ERK-KTR (Regot et al., 2014))
444 expressed in *Xenopus laevis* embryonic spinal cord and muscle cells reports on changes in Erk1/2
445 activity elicited by an agonist or antagonist of the pathway (Figure S1). ERK-KTR is shuttled out
446 of the nucleus when Erk1/2 is activated (Regot et al., 2014). Thus, higher Erk1/2 activity manifests
447 as lower nuclear ERK-KTR signal intensity, while higher nuclear ERK-KTR signal intensity
448 demonstrates inactive Erk1/2 (Figure S1; (Regot et al., 2014)). We find that cells with Ca²⁺

449 transients (Ca^{2+} active) exhibit higher levels of Erk1/2 activity than those cells without Ca^{2+}
450 transients (Ca^{2+} silent) during the recording (Figure 3B). Importantly, VGLuT1-deficient neural
451 plate cells exhibit decreased Erk1/2 activity compared with the wild type counterparts (Figure 3C),
452 suggesting that VGLuT1-mediated glutamate release in the neural plate activates Erk1/2.

453

454 **VGLuT1 is necessary for neural tube formation and regulates neural plate cell proliferation**

455 The data thus far demonstrates that VGLuT1 mediates glutamate release in the folding neural
456 plate that is necessary for recruiting Ca^{2+} signaling during neural tube formation. We therefore
457 investigated the importance of VGLuT1-dependent glutamate release in neural tube closure. By
458 knocking down (Figure 1B) or knocking out (via CRISPR/Cas9) VGLuT1 expression (Figure S2)
459 in developing embryos we find that VGLuT1 deficiency leads to NTDs in *Xenopus laevis* embryos
460 that manifest as failure of closure of the neural tube in the midline (Figure 4). The penetrance of
461 VGLuT1 knockdown-induced NTD phenotype correlates with the extent of knockdown (Figure 1E)
462 and is rescued by restoring VGLuT1 expression (Figure 4), indicating specificity of VGLuT1-KD-
463 elicited NTD phenotype.

464 We find that most VGLuT1-expressing cells are non-proliferative as revealed by the small
465 proportion of VGLuT1/PCNA or VGLuT1/PHH3 co-immunopositive neural plate cells during neural
466 plate folding (Figure 5A). Moreover, overall, a small number of neural plate cells is proliferative in
467 neural plate stage embryos (Fig. 5A). Hence, we examined whether VGLuT1 is necessary for
468 regulating neural plate cell proliferation during neural tube formation. Results show that VGLuT1
469 knockdown increases the number of proliferative cells in the neural plate, evidenced by higher
470 number of total Sox2- and Sox2/PCNA-expressing cells, while there is no significant difference in
471 the number of proliferative cells that do not express Sox2 (Figure 5B). Western blot assays further
472 reveal that VGLuT1 knockdown increases Sox2 expression levels (Figure 5C).

473 Altogether, these results indicate that VGluT1 regulates neural plate cell proliferation and enables
474 neural tube morphogenesis.

475

JNeurosci Accepted Manuscript

476 **Discussion**

477 The vesicular release of neurotransmitter has been primarily studied in the context of chemical
478 synapses between neurons and target cells. Nevertheless, neurotransmitters and their synthetic
479 and release machineries are known to be expressed prior to synapse formation (Lauder et al.,
480 1981; Manent et al., 2005; Root et al., 2008). It could be argued that this precedent is needed for
481 preassembling the specialized molecular platform required in synapses. Alternatively, it could
482 indicate that neurotransmitter signaling plays a critical role even at early stages of nervous system
483 development like the neural plate period. This study demonstrates that the vesicular release of
484 glutamate in the neural plate occurs through mechanisms in part shared by those in synapses,
485 and that this release is indispensable for the formation of the neural tube. These findings attest
486 that expression of glutamate release machinery is not merely preparatory for the synaptogenic
487 period occurring later in development, but that the signaling it elicits is essential for regulating
488 neural cell proliferation during neural plate folding.

489 Here we show expression of components of the vesicular, Ca^{2+} -regulated synaptosomal
490 associated protein receptor (SNARE) complex machinery and VGluT1 immunogold particles
491 localizing to vesicular ultrastructure in the proximity of the apicolateral membrane of neural plate
492 cells. Moreover, we show that glutamate release is VGluT1-dependent and enhanced by Ca^{2+}
493 influx. This suggests that the SNARE-dependent vesicular mechanism is present in neural plate
494 stages. The extent to which this mechanism of vesicular glutamate release resembles the quantal
495 release seen in synapses requires further investigation. Nevertheless, it appears that expression
496 of vesicular release machinery and ultrastructure characteristic of dynamic exocytic and endocytic
497 events, indicative of vesicular release, are staples of the folding neural plate across vertebrates
498 (Portch and Barson, 1974; Takeuchi and Takeuchi, 1980; Shepard et al., 1998; Ybot-Gonzalez
499 and Copp, 1999; Lee and Harland, 2010; Kim and Han, 2011; Ossipova et al., 2014). The
500 morphogenesis of other tissues is also dependent on exocytosis, including the dorsal mesoderm

501 in *Xenopus laevis* (Kreis et al., 2022) and the *Drosophila* air sac primordium (Huang et al., 2019),
502 where vesicular release of glutamate through SNARE-dependent contacts between cytonemes
503 protruding from disc cells and air sac primordium cells has been reported (Huang et al., 2019).
504 Therefore, specialized vesicular glutamate release might be a key mechanism that enables
505 embryonic morphogenesis.

506 Vesicular release is a more energetically demanding process than alternative, non-quantal
507 release mechanisms, but offers more spatiotemporal regulation and organization of the signaling.
508 The presence of this mechanism in neural plate stages suggests that this precision in signaling
509 enabled by the vesicular release of glutamate is important for the specific cellular processes
510 taking place during neural plate folding. Indeed, we find that Ca^{2+} transients, which are strongly
511 dependent on VGluT1-mediated glutamate release, initially occur in individual neural plate cells,
512 with clusters of coactive cells only becoming apparent later in the folding process (Christodoulou
513 and Skourides, 2015; Suzuki et al., 2017; Sequerra et al., 2018). This suggests that the signaling
514 is initially targeted to individual cells during the onset of neural plate folding, allowing for cell
515 autonomy by restricting the release of glutamate to specific cells and subcellular domains.

516 The locally released glutamate and subsequent Ca^{2+} dynamics in individual cells may be
517 necessary for cell-autonomously regulating the cellular behaviors necessary for their participation
518 in the folding of the neural plate. These include decisions on whether a cell should exit the cell
519 cycle to change shape and migrate or continue proliferating to achieve the necessary cell count
520 for neural tube morphogenesis. The VGluT1-dependent Ca^{2+} -Erk1/2 activity that neural plate cells
521 exhibit, demonstrated here, together with previous findings showing that the NTD phenotype from
522 NMDA receptor knockdown is rescued by expressing an inducible, constitutively active MAPK
523 during neural tube formation (Sequerra et al., 2018), suggest that Erk1/2 is downstream
524 glutamate-dependent Ca^{2+} signaling in the regulation of neural plate cell proliferation necessary

525 for neural tube morphogenesis (Figure 6). Nevertheless, further investigation is needed to
526 determine the full downstream signaling and cellular mechanisms of glutamate signaling.

527 Sox2 is a crucial transcription factor for the maintenance of neural cell stemness (Pevny and Rao,
528 2003) by supporting neural stem cell self-renewal in the developing and adult nervous system
529 (Graham et al., 2003; Suh et al., 2007). Its expression is tightly regulated and alterations in this
530 regulation has profound consequences, with constitutive expression inhibiting neuronal
531 differentiation and downregulation leading to premature cell cycle exit and neurogenesis (Graham
532 et al., 2003). We demonstrate that proper Sox2 levels in neural plate cells are dependent on
533 VGlut1 expression which indicates that released glutamate regulates Sox2 expression. This
534 finding reveals a mechanism by which glutamate signaling regulates neural plate cell proliferation.
535 Given that Sox2 expression is negatively correlated to the frequency of Ca^{2+} transients during
536 neural plate folding (Sequerre et al., 2018), it suggests that Ca^{2+} signaling could regulate Sox2
537 levels transcriptionally, as previously shown for Ca^{2+} -dependent regulation of Sox2 expression in
538 *Xenopus* developing neural tube (Shim et al., 2023), and/or post-translationally, through
539 phosphorylation-dependent mechanisms (Lim et al., 2017). We propose a model where VGlut1-
540 dependent, Ca^{2+} mediated release of glutamate in selected neural plate cells signals the need for
541 cells to withdraw from the cell cycle by regulating Sox2 expression, thereby enabling cell shape
542 changes crucial for neural tube morphogenesis (Figure 6).

543 This study underscores the critical role of neural activity and signaling during neural tube
544 formation. Thus, the neural plate and the formation of the neural tube are vulnerable to exposure
545 to environmental factors that can disrupt this neural signaling. Our study provides a foundational
546 understanding of the mechanisms involved in neural tube morphogenesis, which can serve as a
547 mechanistic basis to further investigate how neuroactive drugs interfere with this process, thereby
548 advocating for the cautious use of such therapeutics during pregnancy.

549

550 **References**

- 551 Arriza JL, Eliasof S, Kavanaugh MP, Amara SG (1997) Excitatory amino acid transporter 5, a
552 retinal glutamate transporter coupled to a chloride conductance. *Proc Natl Acad Sci USA*
553 94:4155–4160.
- 554 Balashova OA, Visina O, Borodinsky LN (2017) Folate receptor 1 is necessary for neural plate
555 cell apical constriction during *Xenopus* neural tube formation. *Development* 144:1518–
556 1530.
- 557 Belgacem YH, Borodinsky LN (2011) Sonic hedgehog signaling is decoded by calcium spike
558 activity in the developing spinal cord. *Proc Natl Acad Sci U S A* 108:4482–4487.
- 559 Borodinsky LN, Root CM, Cronin JA, Sann SB, Gu X, Spitzer NC (2004a) Activity-dependent
560 homeostatic specification of transmitter expression in embryonic neurons. *Nature*
561 429:523–530.
- 562 Borodinsky LN, Root CM, Cronin JA, Sann SB, Gu X, Spitzer NC (2004b) Activity-dependent
563 homeostatic specification of transmitter expression in embryonic neurons. *Nature*
564 429:523–530.
- 565 Burger A, Lindsay H, Felker A, Hess C, Anders C, Chiavacci E, Zaugg J, Weber LM, Catena R,
566 Jinek M, Robinson MD, Mosimann C (2016) Maximizing mutagenesis with solubilized
567 CRISPR-Cas9 ribonucleoprotein complexes. *Development:dev*.134809.
- 568 Christodoulou N, Skourides PA (2015) Cell-Autonomous Ca(2+) Flashes Elicit Pulsed
569 Contractions of an Apical Actin Network to Drive Apical Constriction during Neural Tube
570 Closure. *Cell Rep* 13:2189–2202.
- 571 Ciruna B, Jenny A, Lee D, Mlodzik M, Schier AF (2006) Planar cell polarity signalling couples
572 cell division and morphogenesis during neurulation. *Nature* 439:220–224.
- 573 Copp AJ, Brook FA, Roberts HJ (1988a) A cell-type-specific abnormality of cell proliferation in
574 mutant (curly tail) mouse embryos developing spinal neural tube defects. *Development*
575 104:285–295.
- 576 Copp AJ, Crolla JA, Brook FA (1988b) Prevention of spinal neural tube defects in the mouse
577 embryo by growth retardation during neurulation. *Development* 104:297–303.
- 578 Eyal S, Yagen B, Sobol E, Altschuler Y, Shmuel M, Bialer M (2004) The Activity of Antiepileptic
579 Drugs as Histone Deacetylase Inhibitors. *Epilepsia* 45:737–744.
- 580 Graham V, Khudyakov J, Ellis P, Pevny L (2003) SOX2 functions to maintain neural progenitor
581 identity. *Neuron* 39:749–765.
- 582 Hackett JT, Ueda T (2015) Glutamate Release. *Neurochem Res* 40:2443–2460.

583 Haigo SL, Hildebrand JD, Harland RM, Wallingford JB (2003) Shroom induces apical
584 constriction and is required for hinge point formation during neural tube closure. *Curr Biol*
585 13:2125–2137.

586 Harris WA, Hartenstein V (1991) Neuronal determination without cell division in *Xenopus*
587 embryos. *Neuron* 6:499–515.

588 Herrlinger S, Shao Q, Yang M, Chang Q, Liu Y, Pan X, Yin H, Xie L-W, Chen J-F (2019) Lin28-
589 mediated promotion of protein synthesis is critical for neural progenitor cell maintenance
590 and brain development in mice. *Development:dev*.173765.

591 Huang H, Liu S, Kornberg TB (2019) Glutamate signaling at cytoneme synapses. *Science*
592 363:948–955.

593 Jelínek R, Fribová Z (1966) Influence of Mitotic Activity on Neurulation Movements. *Nature*
594 209:822–823.

595 Kaneko S et al. (1999) Congenital malformations due to antiepileptic drugs. *Epilepsy Research*
596 33:145–158.

597 Kim H, Han J (2011) Rab3d is required for *Xenopus* anterior neurulation by regulating noggin
598 secretion. *Developmental Dynamics* 240:1430–1439.

599 Kozak M (1991) Structural features in eukaryotic mRNAs that modulate the initiation of
600 translation. *J Biol Chem* 266:19867–19870.

601 Kreis J, Camuto CM, Elsner CC, Vogel S, Vick P (2022) FGF-mediated establishment of left-
602 right asymmetry requires Rab7 function in the dorsal mesoderm in *Xenopus*. *Front Cell*
603 *Dev Biol* 10:981762.

604 Lauder JM, Wallace JA, Krebs H (1981) Roles for Serotonin in Neuroembryogenesis. In:
605 Serotonin (Haber B, Gabay S, Issidorides MR, Alivisatos SGA, eds), pp 477–506
606 *Advances in Experimental Medicine and Biology*. Boston, MA: Springer US. Available at:
607 http://link.springer.com/10.1007/978-1-4684-3860-4_28 [Accessed May 6, 2023].

608 Lee J-Y, Harland RM (2010) Endocytosis is required for efficient apical constriction during
609 *Xenopus* gastrulation. *Curr Biol* 20:253–258.

610 Leise WF, Mueller PR (2004) Inhibition of the cell cycle is required for convergent extension of
611 the paraxial mesoderm during *Xenopus* neurulation. *Development* 131:1703–1715.

612 Lim S, Bhinghe A, Bragado Alonso S, Aksoy I, Aprea J, Cheok CF, Calegari F, Stanton LW,
613 Kaldis P (2017) Cyclin-Dependent Kinase-Dependent Phosphorylation of Sox2 at Serine
614 39 Regulates Neurogenesis. *Molecular and Cellular Biology* 37:e00201-17.

615 Lindhout D, Omtzigt JG, Cornel MC (1992) Spectrum of neural-tube defects in 34 infants
616 prenatally exposed to antiepileptic drugs. *Neurology* 42:111–118.

617 Manent JB, Demarque M, Jorquera I, Pellegrino C, Ben-Ari Y, Aniksztejn L, Represa A (2005) A
618 noncanonical release of GABA and glutamate modulates neuronal migration. *J Neurosci*
619 25:4755–4765.

620 Marvin JS, Borghuis BG, Tian L, Cichon J, Harnett MT, Akerboom J, Gordus A, Renninger SL,
621 Chen T-W, Bargmann CI, Orger MB, Schreiter ER, Demb JB, Gan W-B, Hires SA,
622 Looger LL (2013) An optimized fluorescent probe for visualizing glutamate
623 neurotransmission. *Nat Methods* 10:162–170.

624 McShane SG, Molè MA, Savery D, Greene NDE, Tam PPL, Copp AJ (2015) Cellular basis of
625 neuroepithelial bending during mouse spinal neural tube closure. *Developmental Biology*
626 404:113–124.

627 Moreno-Mateos MA, Vejnar CE, Beaudoin J-D, Fernandez JP, Mis EK, Khokha MK, Giraldez AJ
628 (2015) CRISPRscan: designing highly efficient sgRNAs for CRISPR-Cas9 targeting in
629 vivo. *Nat Methods* 12:982–988.

630 Nakagawa S, Niimura Y, Gojobori T, Tanaka H, Miura K -i. (2007) Diversity of preferred
631 nucleotide sequences around the translation initiation codon in eukaryote genomes.
632 *Nucleic Acids Research* 36:861–871.

633 Nakane Y et al. (1980) Multi-institutional Study on the Teratogenicity and Fetal Toxicity of
634 Antiepileptic Drugs: A Report of a Collaborative Study Group in Japan. *Epilepsia*
635 21:663–680.

636 Namimatsu S, Ghazizadeh M, Sugisaki Y (2005) Reversing the Effects of Formalin Fixation with
637 Citraconic Anhydride and Heat: A Universal Antigen Retrieval Method. *J Histochem*
638 *Cytochem* 53:3–11.

639 Nieuwkoop PD, Faber J (1994) Normal table of *Xenopus laevis* (Daudin): a systematical and
640 chronological survey of the development from the fertilized egg till the end of
641 metamorphosis. New York: Garland Pub.

642 Nikolopoulou E, Galea GL, Rolo A, Greene NDE, Copp AJ (2017) Neural tube closure: cellular,
643 molecular and biomechanical mechanisms. *Development* 144:552–566.

644 Omtzigt JG, Los FJ, Grobbee DE, Pijpers L, Jahoda MG, Brandenburg H, Stewart PA, Gaillard
645 HL, Sachs ES, Wladimiroff JW (1992) The risk of spina bifida aperta after first-trimester
646 exposure to valproate in a prenatal cohort. *Neurology* 42:119–125.

647 Ossipova O, Kim K, Lake BB, Itoh K, Ioannou A, Sokol SY (2014) Role of Rab11 in planar cell
648 polarity and apical constriction during vertebrate neural tube closure. *Nat Commun*
649 5:3734.

650 Parchem RJ, Moore N, Fish JL, Parchem JG, Braga TT, Shenoy A, Oldham MC, Rubenstein
651 JLR, Schneider RA, Blelloch R (2015) miR-302 Is Required for Timing of Neural
652 Differentiation, Neural Tube Closure, and Embryonic Viability. *Cell Reports* 12:760–773.

653 Park TJ, Gray RS, Sato A, Habas R, Wallingford JB (2005) Subcellular localization and
654 signaling properties of dishevelled in developing vertebrate embryos. *Curr Biol* 15:1039–
655 1044.

656 Pevny L, Rao MS (2003) The stem-cell menagerie. *Trends in Neurosciences* 26:351–359.

657 Pokrovsky D, Forné I, Straub T, Imhof A, Rupp RAW (2021) A systemic cell cycle block impacts
658 stage-specific histone modification profiles during *Xenopus* embryogenesis Misteli T, ed.
659 *PLoS Biol* 19:e3001377.

660 Portch PA, Barson AJ (1974) Scanning electron microscopy of neurulation in the chick. *J Anat*
661 117:341–350.

662 Regot S, Hughey JJ, Bajar BT, Carrasco S, Covert MW (2014) High-Sensitivity Measurements
663 of Multiple Kinase Activities in Live Single Cells. *Cell* 157:1724–1734.

664 Root CM, Velazquez-Ulloa NA, Monsalve GC, Minakova E, Spitzer NC (2008) Embryonically
665 expressed GABA and glutamate drive electrical activity regulating neurotransmitter
666 specification. *J Neurosci* 28:4777–4784.

667 Sequerra EB, Goyal R, Castro PA, Levin JB, Borodinsky LN (2018) NMDA Receptor Signaling
668 Is Important for Neural Tube Formation and for Preventing Antiepileptic Drug-Induced
669 Neural Tube Defects. *J Neurosci* 38:4762–4773.

670 Session AM et al. (2016) Genome evolution in the allotetraploid frog *Xenopus laevis*. *Nature*
671 538:336–343.

672 Shcherbakova DM, Verkhusa VV (2013) Near-infrared fluorescent proteins for multicolor in
673 vivo imaging. *Nat Methods* 10:751–754.

674 Shen MW, Arbab M, Hsu JY, Worstell D, Culbertson SJ, Krabbe O, Cassa CA, Liu DR, Gifford
675 DK, Sherwood RI (2018) Predictable and precise template-free CRISPR editing of
676 pathogenic variants. *Nature* 563:646–651.

677 Shepard TH, Muffley LA, Thayer Smith L (1998) Ultrastructural study of mitochondria and their
678 cristae in embryonic rats and primate (*N. nemestrina*). *Anat Rec* 252:383–392.

679 Shim S, Goyal R, Panoutsopoulos AA, Balashova OA, Lee D, Borodinsky LN (2023) Calcium
680 dynamics at the neural cell primary cilium regulate Hedgehog signaling-dependent
681 neurogenesis in the embryonic neural tube. *Proc Natl Acad Sci USA* 120:e2220037120.

682 Suh H, Consiglio A, Ray J, Sawai T, D'Amour KA, Gage FH (2007) In Vivo Fate Analysis
683 Reveals the Multipotent and Self-Renewal Capacities of Sox2+ Neural Stem Cells in the
684 Adult Hippocampus. *Cell Stem Cell* 1:515–528.

685 Suzuki M, Sato M, Koyama H, Hara Y, Hayashi K, Yasue N, Imamura H, Fujimori T, Nagai T,
686 Campbell RE, Ueno N (2017) Distinct intracellular Ca²⁺ dynamics regulate apical
687 constriction and differentially contribute to neural tube closure.
688 *Development*:dev.141952.

689 Swapna I, Borodinsky LN (2012) Interplay between electrical activity and bone morphogenetic
690 protein signaling regulates spinal neuron differentiation. *Proc Natl Acad Sci U S A*
691 109:16336–16341.

692 Sweatt JD (2004) Mitogen-activated protein kinases in synaptic plasticity and memory. *Current*
693 *Opinion in Neurobiology* 14:311–317.

694 Takeuchi YK, Takeuchi IK (1980) ULTRASTRUCTURAL CHANGES IN EMBRYONIC
695 ECTODERMAL CELLS OF THE NEURULATING RAT EMBRYO. *Dev Growth Differ*
696 22:627–637.

697 Thomas GM, Huganir RL (2004) MAPK cascade signalling and synaptic plasticity. *Nat Rev*
698 *Neurosci* 5:173–183.

699 Wallingford JB, Niswander LA, Shaw GM, Finnell RH (2013) The continuing challenge of
700 understanding, preventing, and treating neural tube defects. *Science* 339:1222002.

701 Werler MM, Ahrens KA, Bosco JLF, Mitchell AA, Anderka MT, Gilboa SM, Holmes LB (2011)
702 Use of Antiepileptic Medications in Pregnancy in Relation to Risks of Birth Defects.
703 *Annals of Epidemiology* 21:842–850.

704 Wlodarczyk BJ, Palacios AM, George TM, Finnell RH (2012) Antiepileptic drugs and pregnancy
705 outcomes. *Am J Med Genet* 158A:2071–2090.

706 Yang S-L, Yang M, Herrlinger S, Liang C, Lai F, Chen J-F (2015) MiR-302/367 regulate neural
707 progenitor proliferation, differentiation timing, and survival in neurulation. *Developmental*
708 *Biology* 408:140–150.

709 Ybot-Gonzalez P, Cogram P, Gerrelli D, Copp AJ (2002) Sonic hedgehog and the molecular
710 regulation of mouse neural tube closure. *Development* 129:2507–2517.

711 Ybot-Gonzalez P, Copp AJ (1999) Bending of the neural plate during mouse spinal neurulation
712 is independent of actin microfilaments. *Dev Dyn* 215:273–283.

713 Zhou Y, Danbolt NC (2014) Glutamate as a neurotransmitter in the healthy brain. *J Neural*
714 *Transm* 121:799–817.

715

716 **Figure legends**

717 **Figure 1. VGluT1 is expressed in the neural plate of *Xenopus laevis* embryos.** (A-D) RNA
718 was isolated from embryos at mid-neural plate stages and reverse transcriptase (RT)-PCR assays
719 were performed for *vglut1*, *eeat5*, *syntaxin1a (stx1a)*, *vamp1* and *snap25*. (B) Embryos were
720 injected with a splicing-blocking morpholino targeting *vglut1* (VGluT1-KD2) or control morpholino
721 (Control). RT-PCR was performed with primers flanking a sequence between exon 1 and 2, that
722 can only be detected in correctly spliced transcript (control). Shown is representative example of
723 RT-PCR product in control and VGluT1-KD2 samples, N=3. (C-D) Quantitative RT-PCR was
724 performed from samples of embryos at stage 20 to compare relative expression of *vglut1*, *vglut2*
725 and *vglut3* (C) or with embryos at stages (st.) 13, 15, 17 and 20 to compare developmental
726 regulation of *vglut1* during neural plate folding (D). Graphs show individual and mean \pm SEM
727 transcript level as ratio of control transcript (sub-1, C) or as percent of *vglut1* transcript level in
728 the youngest stage tested (st. 13, D). N=4 (D) and 3(C) experiments, * $p < 0.05$, ** $p < 0.01$,
729 *** $p < 0.001$, one-way ANOVA (C and D), and one-sample t and Wilcoxon test (D, compared to
730 hypothetical value of 1 (st. 13)). (E) Western blot assays were performed in whole-cell lysates
731 from neural-plate-stage control, VGluT1-knockdown (KD) and *vglut1* mRNA-injected embryos.
732 GAPDH was used as loading normalizer. Shown is a representative example. Graph shows
733 normalized signal intensities from individual samples and means as percentages of control values
734 (dashed line) from $N \geq 4$ experiments. Statistical analysis was done with one-sample t and
735 Wilcoxon test, ** $p < 0.01$, **** $p < 0.0001$. (F) Representative maximum intensity projection of whole-
736 mount immunostained dorsal half of mid-neural plate stage (st. 16) embryo for VGluT1 and Sox2
737 (neural stem cell marker). Graphs show mediolateral (left; mean percent of VGluT1+ cells per
738 100-mm bin from the midline compared to the total number of VGluT1+ cells \pm SEM) or
739 developmental (right; individual data and mean percent of VGluT1+ cells of the total number of
740 Sox2+ cells \pm SEM) distribution of number of VGluT1 immunopositive (+) cells. ** $p < 0.01$, ns: not

741 significant, one-way ANOVA. N=3. (G) VGluT1-KD decreases the number of VGluT1+ cells in the
742 neural plate. Shown is a maximum intensity projection of whole-mount immunostained unilaterally
743 VGluT1-KD neural plate from a representative embryo, N=3. (H) Representative maximum
744 intensity projection of 10 mm-thick transverse section of neural plate stage (st. 16) embryo for
745 VGluT1 and b-tubulin, nuclei labeled with DAPI. Scale bars, 20 μ m. (I-K) Neural plate stage (st.
746 18) embryos were processed for transmitted (I) and immuno-transmitted (J-K) electron
747 microscopy assays. Shown are representative examples. A: apical, B: basal. Dashed boxes in (I-
748 K) indicate fields of view shown in (I'-K'). Arrow in (I') points to vesicular structures and in (J') to
749 structure with lipidic-looking background (vesicular) close to the cell-cell border immunopositive
750 for VGluT1. (J-K) Ultrathin embryos sections were incubated with (J-J') or without (K-K') 1:3,000
751 VGluT1 antibody, followed by the same immunogold labeling procedure as indicated in Materials
752 and Methods. N=3, scale bars, 2 (I-K) and 0.2 (I'-K') μ m.

753

754 **Figure 2. Glutamate is released from neural plate stage embryos in a VGluT1- and Ca²⁺-**
755 **dependent manner.** (A-E) Two-cell stage embryos were bilaterally microinjected with mRNA
756 encoding iGluSnFR (A-E) or membrane (memb)-mCherry (B-C) and unilaterally injected with
757 VGluT1-morpholino 1 (VGluT1-knockdown (KD), C-D) or control-morpholino (Control, C).
758 Embryos were live imaged (A-C, E) or processed for immunostaining (D). (A) iGluSnFR
759 expressed in neural plate stage embryos senses extracellular glutamate levels. Shown are single
760 time frames of time-lapse recording of the neural plate in whole embryo when either vehicle or 5
761 mM glutamate was added to the bathing solution. Trace shows representative change in
762 iGluSnFR fluorescence intensity over time. Graph shows individual maximal change in iGluSnFR
763 fluorescence intensity after addition of vehicle or 5 mM glutamate. N=7, **p<0.01, ns: not
764 significant, paired ANOVA. (B) Released glutamate is higher in the neural plate. Shown is
765 maximum intensity projection of confocal image of iGluSnFR or memb-mCherry-expressing

766 embryos and mediolateral fluorescence intensity profile for both reporters. While iGluSnFR
767 exhibits higher intensity in membrane of neural plate cells located within 200 μ m of the midline
768 compared to non-neural ectodermal cells, memb-mCherry does not show a differential
769 mediolateral distribution. Graphs show example (B'), all individual experiments (B'', B''') and
770 mean+SD (B''') mediolateral iGluSnFR and memb-mCherry fluorescence intensity (B') and percent
771 intensity profile (B''-B'''), N=5 iGluSnFR- and N=4 memb-mCherry-expressing embryos.
772 Comparison of best fit curves for iGluSnFR and memb-mCherry shows significantly different
773 fluorescence intensity profiles (B''', **** $p < 0.0001$, non-linear regression fit, Lorentzian (Cauchy)).
774 (C) VGluT1-KD impairs glutamate release. Images are representative examples of maximum
775 intensity projection of unilaterally manipulated embryos as indicated. Graphs represent iGluSnFR
776 (left and middle) or memb-mCherry (right) fluorescence intensity of individual embryos in WT and
777 manipulated halves of neural plate. *** $p < 0.001$, ns: not significant, N=5 (VGluT1-KD iGluSnFR
778 and memb-mCherry), N=6 (Control), 2-tail paired t-test. (D) Expression of iGluSnFR is not
779 affected by VGluT1-KD. Shown is a representative example of 10 μ m section of unilaterally
780 VGluT1-KD neural plate immunostained for myc-tag linked to iGluSnFR construct, N=3. (E) Ca^{2+}
781 entry in neural plate cells increases glutamate release. Images show iGluSnFR expressing neural
782 plate before and after addition of 5 mM ionomycin. Graph shows individual data of % maximal
783 change in iGluSnFR fluorescence intensity after addition of ionomycin. N=4, * $p < 0.05$, one-sample
784 t and Wilcoxon test, compared to the hypothetical value of 100 (before addition of ionomycin). (F-
785 H) Neural plate stage wildtype (F,H) and bilaterally morpholino-injected embryos (G, Control and
786 VGluT1-KD) were incubated with 2 mM ionomycin (F-H) or vehicle (F) in the presence (H) or
787 absence (F-H) of 100 nM tetanus toxin for 20 min. Bathing solution was collected and released
788 glutamate measured with a Fluorometric Glutamate Assay Kit. (F) Graph shows released
789 glutamate concentration in Control (vehicle) and ionomycin treated embryos, N=9, ** $p < 0.01$, 2-
790 tail paired t-test. (G) Graph shows individual % change in released glutamate concentration in
791 Control and VGluT1-KD embryos treated with ionomycin and compared to vehicle-treated (100%),

792 N=4, *p<0.05, 2-tail paired t-test. (H) Graph shows individual % change in released glutamate
793 concentration in embryos treated with ionomycin in the absence or presence of 100 nM tetanus
794 toxin compared to untreated (100%), N=6, *p<0.05, 2-tail paired t-test.

795

796 **Figure 3. Ca²⁺ dynamics in the neural plate during folding depend on VGluT1 and activate**

797 **Erk1/2.** (A) Two-cell-stage embryos were unilaterally VGluT1 knocked down (KD) and bilaterally

798 injected with mRNA encoding GCaMP6s, Ca²⁺ reporter. Neural plate stage embryos were

799 timelapse imaged for 5 min and number of Ca²⁺ transients were measured. Image shows

800 representative example of unilateral (red) VGluT1-KD and Control embryos. Circled cells are

801 those exhibiting Ca²⁺ transients during recording. Graphs show individual number of Ca²⁺

802 transients per 5 min in WT and VGluT1-KD or Control halves of the neural plate. N=6 VGluT1-KD

803 and 5 Control embryos, *p<0.05, ns: not significant, 2-tail paired t-test. (B) Two-cell stage embryos

804 were bilaterally injected with ERK-KTR-iRFP670 (Erk1/2 activity reporter), H2B-RFP (nuclear

805 marker), and GCaMP6s. Neural-plate-stage embryos were time-lapse imaged for 2 h, and cells

806 exhibiting Ca²⁺ transients and those matching contralaterally their mediolateral and

807 anteroposterior locations were selected for measurement of the ERK-KTR nuclear (delimited by

808 H2B signal) and non-nuclear (cytosolic, delineated by GCaMP6 signal) fluorescence signal. ERK-

809 KTR reports on active and inactive Erk1/2 with low and high nuclear versus cytosolic fluorescence

810 intensity, respectively (Figure S1). Upper images are a representative example of single time

811 frame of an embryo live-imaged. Cyan arrows point to two cells exhibiting Ca²⁺ transients (active),

812 and white arrows point to similarly positioned (mediolaterally and anteroposteriorly) cells that did

813 not exhibit Ca²⁺ transients (silent) during recording. Bottom images show the two cells exhibiting

814 Ca²⁺ transients during peak of transient. Graph shows mean ratio of ERK-KTR cytosolic/nuclear

815 fluorescence intensity per embryo in active and silent cells. N=7 embryos, n=10 cells per embryo,

816 **p<0.01, 2-tail paired t-test. (C) Two-cell stage embryos were bilaterally injected with ERK-KTR-

817 iRFP670 and H2B-RFP, and unilaterally with VGluT1-KD or Control along with tracer. Neural plate
818 stage embryos were time-lapse imaged and ERK-KTR nuclear (delimited by H2B signal) and
819 cytosolic fluorescence signal was measured in WT and injected neural plate cells. Images show
820 single time frame of unilateral VGluT1-KD and Control embryos. Yellow line separates WT from
821 injected half neural plate. Graph shows mean ratio of ERK-KTR cytosolic/nuclear fluorescence
822 intensity in each half of the neural plate per embryo. N=4 embryos, n=10 cells per embryo
823 (VGluT1-KD) and N=5 embryos, n=10 cells per embryo (Control), **p<0.01, ns: not significant,
824 two-tail paired t-test.

825

826 **Figure 4. VGluT1 is necessary for neural tube formation.** Two (A) or 8 (B)-cell stage embryos
827 were bilaterally (A-B) and dorsal blastomeres only (B) injected with 2-8 (A) or 2 (B) pmol VGluT1-
828 morpholino 1 translation-blocking (VGluT1-KD1), 8 pmol VGluT1-morpholino 2 splicing-blocking
829 (VGluT1-KD2, A) or 8 (A) or 2 (B) pmol control-morpholino (Control) without (A,B) or with (A)
830 morpholino-resistant *vglut1* mRNA, or with Cas9 or Cas9 + VGluT1 sgRNA (VGluT1-KO, A).
831 Images (A, brightfield images in B) show representative examples of embryos at the time neural
832 tube closed in Control group. Red arrows indicate open neural tube. Fluorescence images in (B)
833 indicate neural tissue-specific targeting of Control and VGluT1-KD. Graphs show % of embryos
834 with open and closed neural tubes in each group. N_≥5 (A) and N=3 (B) experiments, n of embryos
835 indicated in graph for each group, *p<0.05, **p<0.01, ***p<0.001, ****p<0.0001, ns: not significant,
836 one-way ANOVA, mixed-effects analysis with Geisser-Greenhouse correction, Dunnett's multiple
837 comparisons test, compared to WT (A) or two-tail paired t-test (B).

838

839 **Figure 5. VGluT1 regulates neural plate cell proliferation and Sox2 expression.** (A) Wild type
840 neural plate stage (st. 18) embryos were processed for whole-mount immunostaining for VGluT1,

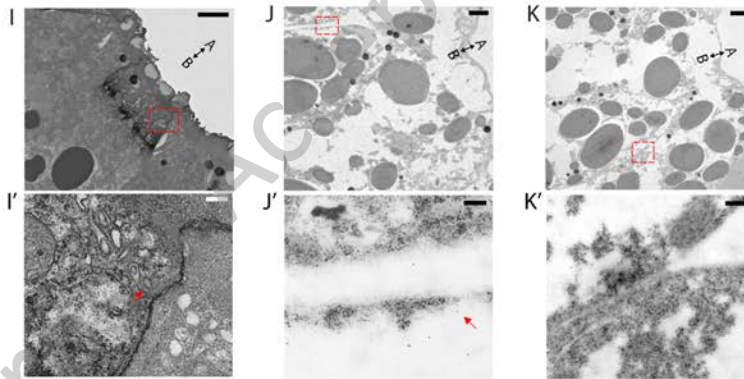
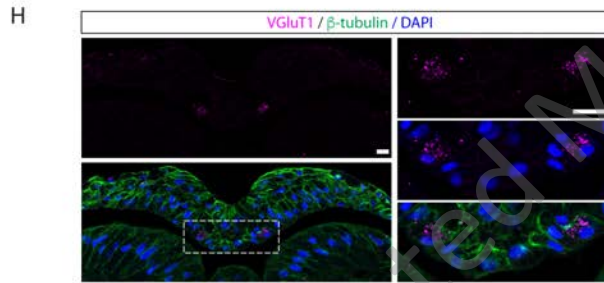
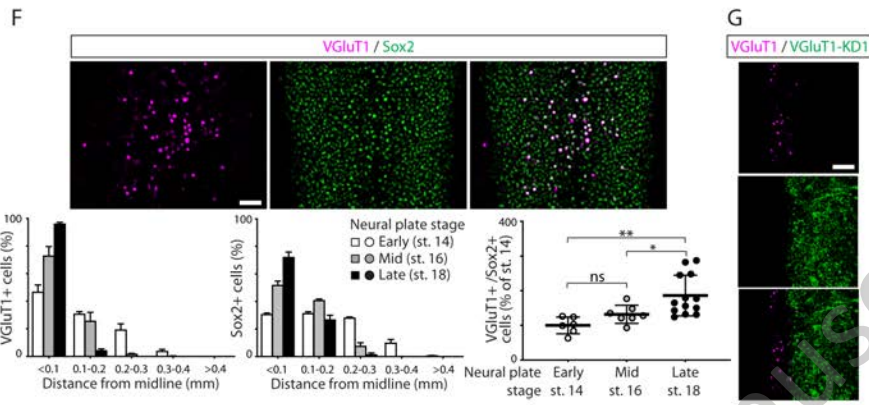
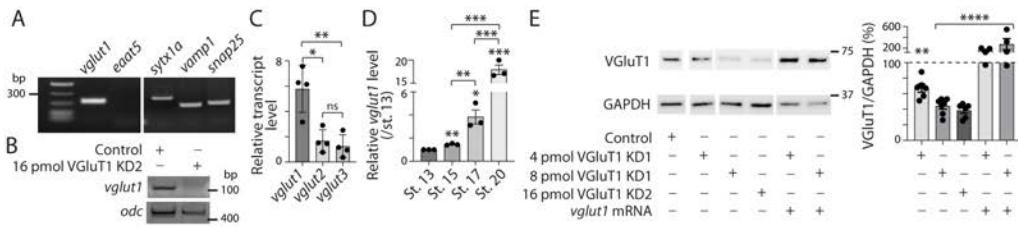
841 Sox2 and cell proliferation markers PCNA and PHH3. Shown are representative images. Graph
842 shows individual and mean \pm SD number of total and proliferation marker immunopositive VGlut1
843 neural plate cells (Sox2+). (B) Two-cell stage embryos were unilaterally injected with VGlut1-KD
844 along with tracer. Neural plate stage (st. 18) embryos were processed for immunostaining.
845 Images show representative example. Graphs show individual number of immunopositive (+) cells
846 in both halves of the neural plate per embryo. N=7 embryos, **p<0.01, ***p<0.001, ns: not
847 significant, 2-tail paired t-test. (C) Two-cell stage embryos were bilaterally injected with VGlut1-
848 KD or Control. Neural plate stage embryos were processed for Western blot assays for Sox2 and
849 GAPDH, as loading control. Image is a representative example. Graph shows individual samples
850 and mean \pm SD normalized Sox2 levels. N=5 experiments, **p<0.01, 2-tail t-test.

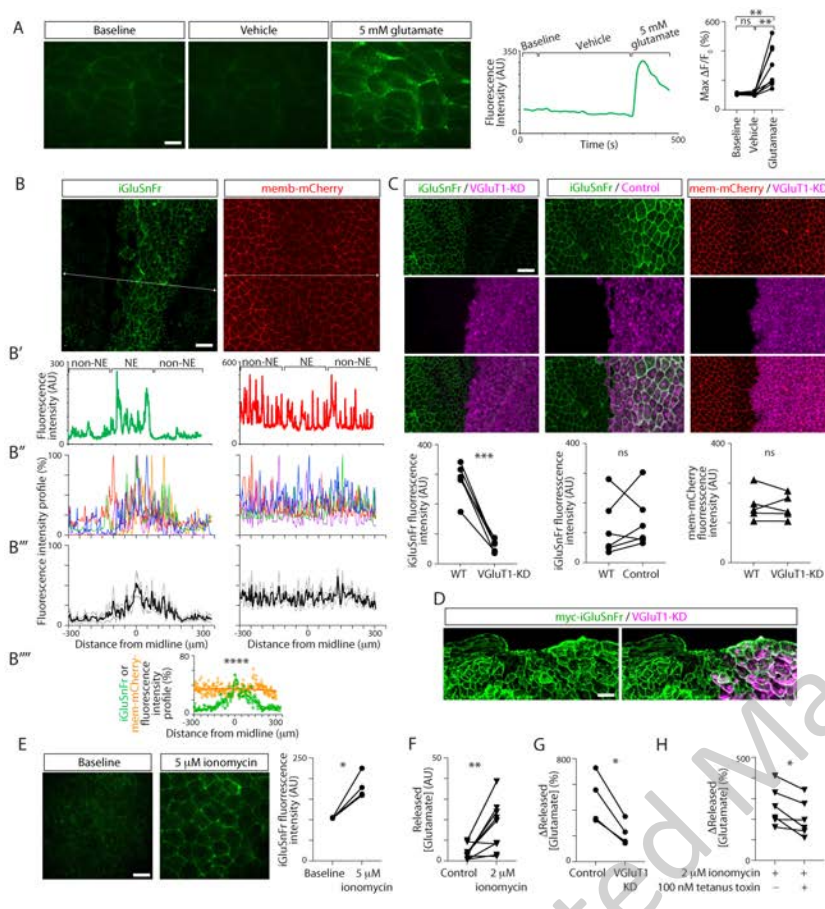
851

852 **Figure 6. Model of mechanism of VGlut1-dependent regulation of neural tube formation.**

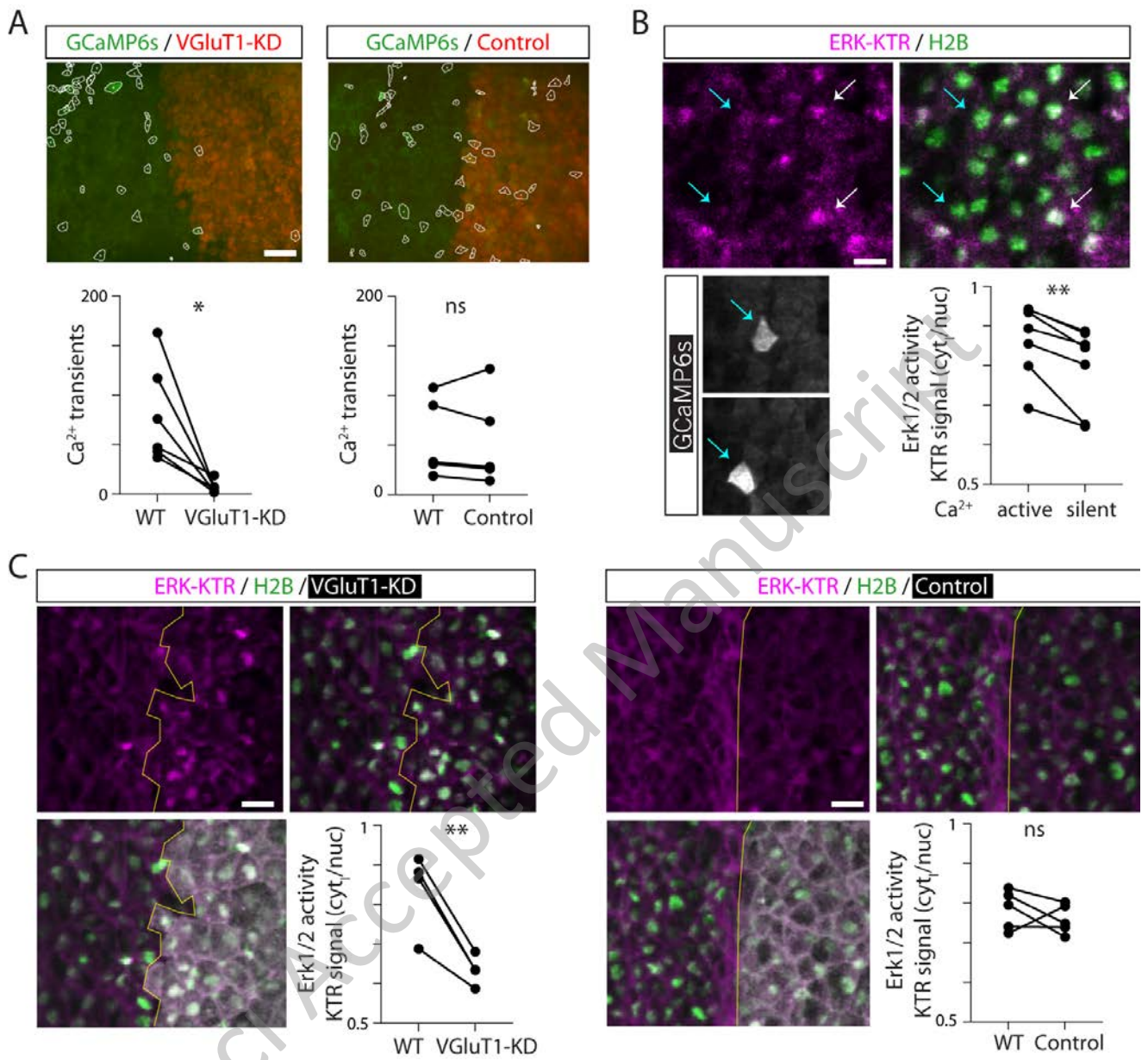
853 Vesicular release of glutamate (1) activates glutamate receptors eliciting Ca²⁺ transients in neural
854 plate cells (2), which are necessary for the regulation of neural plate cell proliferation by
855 downregulating Sox2 expression potentially (dashed arrows) through the recruitment of Erk1/2
856 (3) and/or other signaling pathways (4). Ca²⁺ transients are also necessary for the changes in cell
857 shape (5) required for the timely folding of the neural plate during neural tube morphogenesis.

858

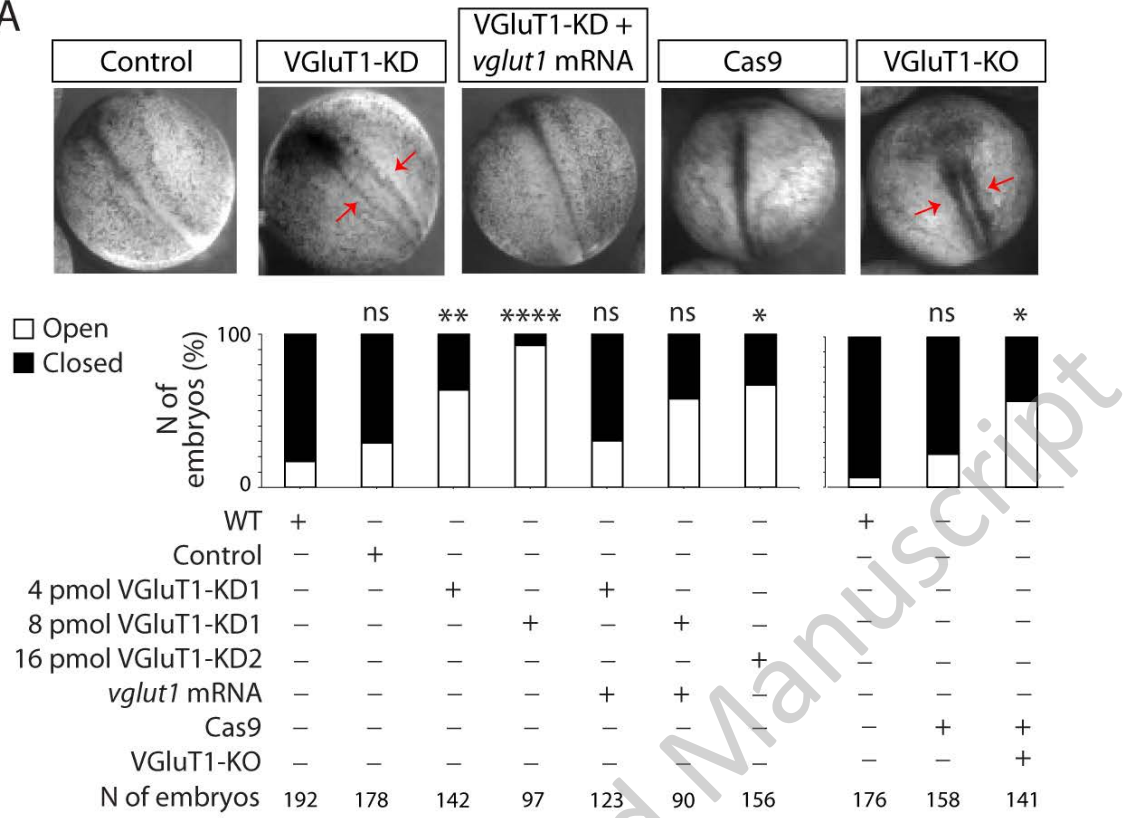




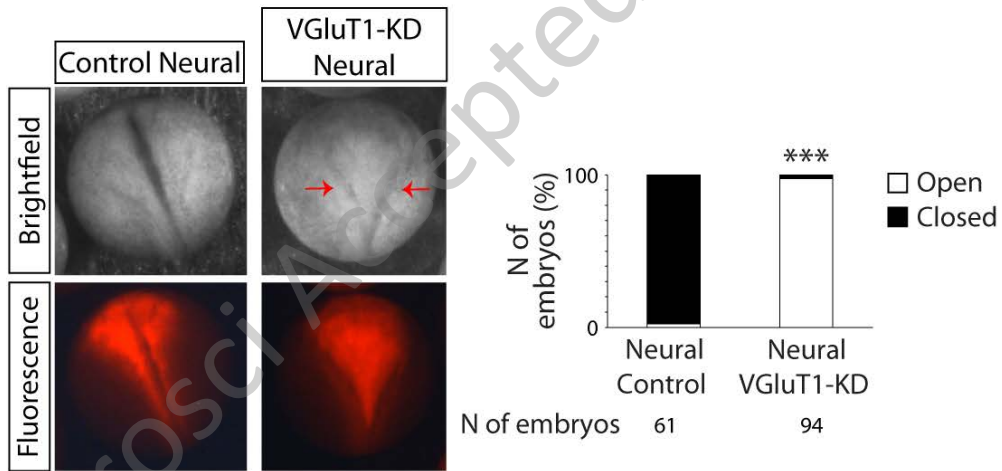
JNeurosci Accepted Manuscript

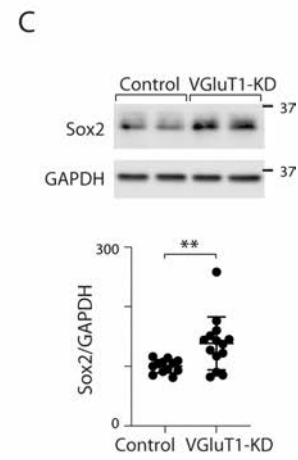
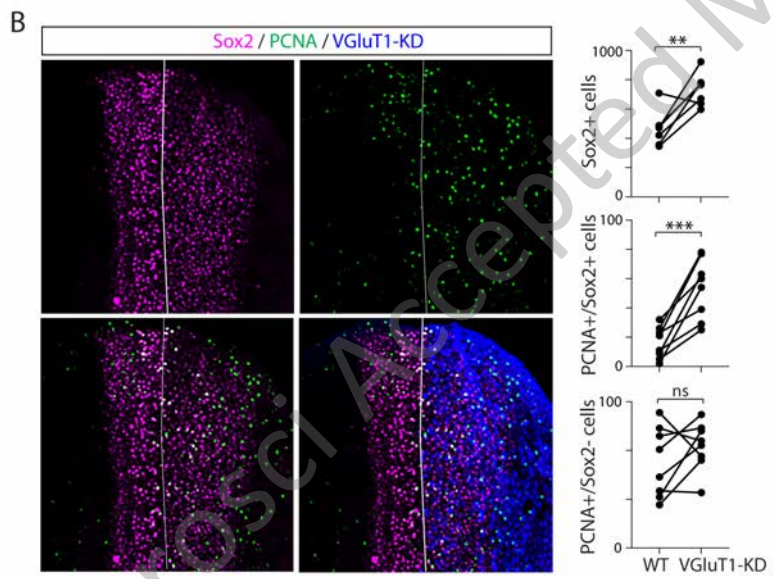
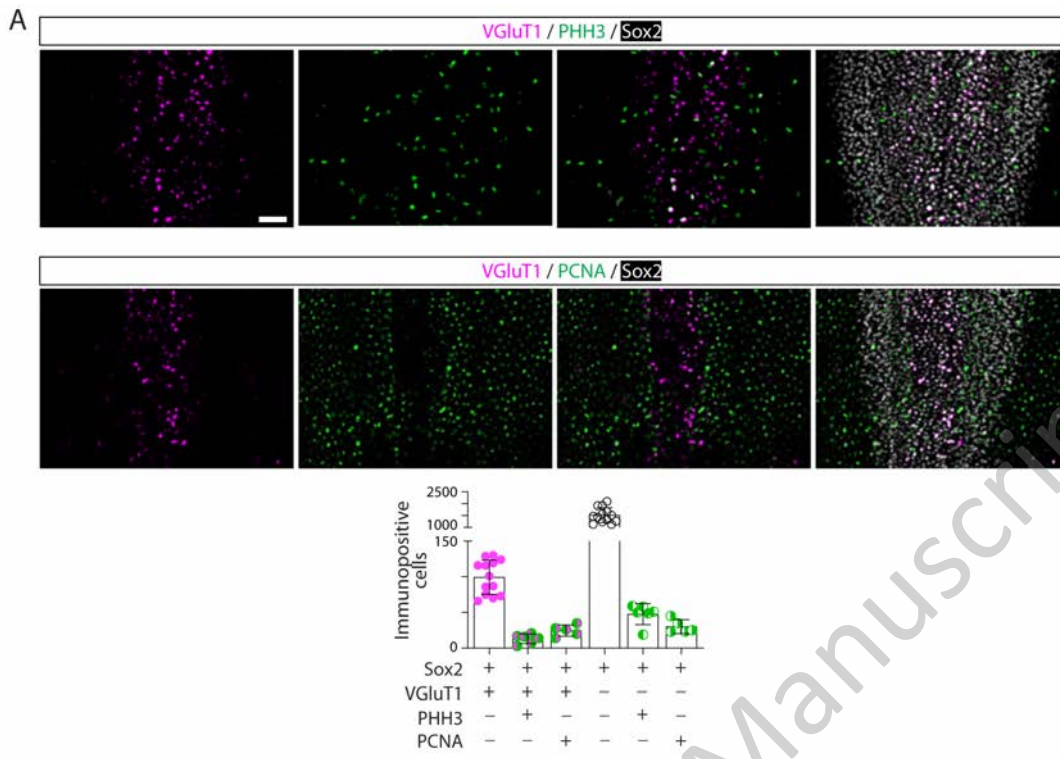


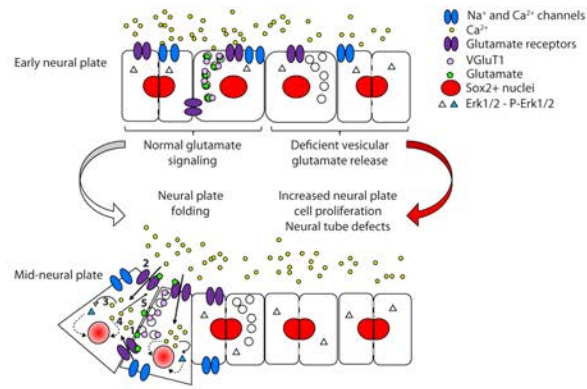
A



B







JNeurosci Accepted Manuscript